ACS APPLIED MATERIALS & INTERFACES

Research Article

Cite This: ACS Appl. Mater. Interfaces XXXX, XXX, XXX−XXX

www.acsami.org

Multilayer Functional Tapes Cofired at 450 °C: Beyond HTCC and LTCC Technologies

Jobin Varghese,* Tuomo Siponkoski, Maciej Sobocinski, Timo Vahera, and Heli Jantunen

Microelectronics Research Unit, Faculty of Information Technology and Electrical Engineering, University of Oulu, FI-90014 Oulu, Finland

Supporting Information

ABSTRACT: This paper reports the first ultralow sintering temperature (450 °C) cofired multifunctional ceramic substrate based on a commercial lead zirconium titanate (PZ29)−glass composite, which is fabricated by tape casting, isostatic lamination, and sintering. This substrate was prepared from a novel tape casting slurry composition suitable for cofiring at low temperatures with commercial Ag electrodes at 450 °C. The green cast tape and sintered substrate showed a surface roughness of 146 and 355 nm, respectively, suitable for device-level fabrication by postprocessing. Additionally, the ferroelectric and piezoelectric studies disclosed low remnant polarization due to the dielectric glass matrix with average values of piezoelectric coefficient ($+d_{33}$) and voltage coefficient ($+g_{33}$) of 17 pC/N and 30 mV/N, respectively. The dielectric permittivity and loss value of the sintered substrates were 57.8 and 0.05 respectively, at 2.4 GHz. The variation of relative permittivity on temperature dependence in the range of −40 to 80 °C was about 23%, while the average linear coefficient of thermal expansion was 6.9 ppm/°C in the measured temperature range of 100−300 °C. Moreover, the shelf life of the tape over 28 months was studied through measurement of the stability of the dielectric properties over time. The obtained results open up a new strategy for the fabrication of next-generation low-cost functional ceramic devices prepared at an ultralow temperature in comparison to the high-temperature cofired ceramic and low-temperature cofired ceramic technologies.

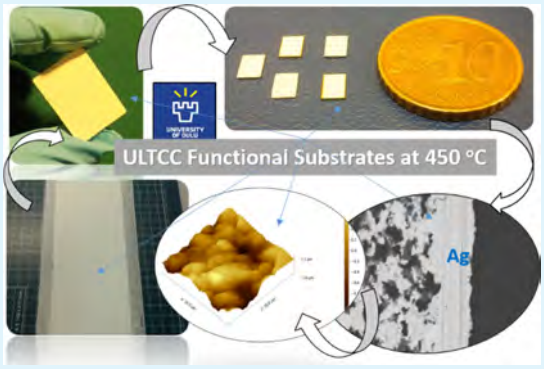

KEYWORDS: *ULTCC, tape casting, cofiring, dielectric properties, functional properties, CTE*

1. INTRODUCTION

Decreasing the sintering temperature of ceramics is attracting more and more attention for the fabrication of next-generation low-cost ceramic products such as multichip modules,[1] substrates,[2] packages,[3] and functional micro-electro mechanical systems.[4,5] The ultralow temperature cofired ceramics (ULTCC) technology, especially, has progressed rapidly.[6−11] The ULTCC concept is nucleated from the conventional high-temperature cofired ceramic (HTCC) and low-temperature cofired ceramic (LTCC) technologies.[12−14] The ULTCC technology has been a hot topic since 2015,[15−17] although the first material's composition was reported by Udovic et al. in 2001.[18] To date, over 200 ULTCC material compositions have been reported and have been divided into two categories: I (fabrication close to room temperature) and II (fabrication at 400−700 °C) based on the processing conditions.[12] So far, there have been only a few devices developed based on this concept,[19] although several materials with outstanding dielectric properties suitable for microwave telecommunication applications are reported.[13,20] In addition to microwave materials, functional ceramics such as piezoelectrics are also technologically important because of their broad areas of application covering different sensing solutions, acoustic emission, sonars, flow meters, acceleration, dynamic force measurements, and fuel level meters and, most recently, energy-harvesting solutions.[21]

Lead zirconium titanate ($PbZr_xTi_{1-x}O_3$, PZT) is the most well-known and widely used commercial piezoelectric material. There are several commercially available piezoelectric ceramics; PZ29, for example, has very high coupling factors and piezoelectric charge coefficients designed especially for high sensitivity or displacement applications.[22] Most of the PZT ceramics have sintering temperatures in the range of 1250−1350 °C.[23] However, to the best of our knowledge, no piezoelectric composition with a sintering temperature below 500 °C has been reported, except for polymer-based composites and inks.[24,25] The ULTCC approach for piezoelectric materials would also be extremely beneficial offering low-cost processing route with decreased thermal, mechanical, and microstructural challenges, and most importantly, needing no protection against Pb volatilization. Unlike in the case of LTCC and HTCC, the low fabrication temperature of ULTCCs, especially when being below 500 °C, does not cause the volatilization of lead. This reduces the toxicity in the

Received: January 18, 2018
Accepted: March 7, 2018
Published: March 7, 2018

DOI: 10.1021/acsami.8b00978
ACS Appl. Mater. Interfaces XXXX, XXX, XXX−XXX

Figure 1. Tape casting processing flow chart.

fabrication step. Cost effectiveness on the other hand is achieved through lower energy consumption because of the lower fabrication temperature and low-cost investments for firing-furnaces. The present paper describes the first attempt to develop a functional PZT−glass-based ULTCC composition by tape casting and cofiring at 450 °C.

However, to the extent of our knowledge, we presented the very first functional ULTCC tape characterized in both radio and microwave frequency ranges along with functional properties and cofirability with commercial Ag electrodes. It is worth noting that even in the cases of LTCC and HTCC, most of the compositions reported have low permittivity and low dielectric loss and are meant for passive microwave components and packages.[12,13] The developed ULTCC material has a wide range of applications in the field of multilayer packages with better overall stability than the polymer−ceramic composites. However, the present ULTCC still needs further research to improve the electrical performance more feasible for practical functional applications.

2. MATERIALS AND METHODS

2.1. Materials and Their Process. The proposed ULTCC composite is based on equal amounts in wt % (0.56 volume fraction of PZ29 and 0.44 volume fraction of commercial glass) of commercial PZ29 (Ferro perm Piezoceramics A/S) ceramic and low melting-point sealing glass (Go17, SCHOTT technical glasses with Pb_2O_3, Li_2O, Al_2O_3, and Si_2O), that was prepared by conventional ball milling for 12 h. The particle size and surface area analyses of the powder were performed using the laser diffraction method (Beckman Coulter LS13320) and a particle surface area analyzer (G.W. Berg & Co. Micromeritics ASAP 2020).

Figure 1 shows the detailed fabrication flow chart of this process. The PZ29−glass composite powder was mixed with dimethyl carbonate (DMC; Sigma-Aldrich, St. Louis, MO) as a solvent and poly(propylene carbonate) (QPAC40; Empower Materials, New Castle, DE) as a binder by milling for 12 h. After the addition of the two plasticizers, butyl benzyl phthalate (S160; Richard E. Mistler, Yardley, Pennsylvania) and polyethylene glycol (UCON 50HB2000; Richard E. Mistler), the milling was further continued for 24 h. The resultant slurry was cast on a silicone-coated Mylar carrier tape using a 200 μm gap under the doctor blade and a laboratory caster (Unicaster 2000, Leeds, U.K.) at a speed of 0.8 m/min. The green tape was peeled from the Mylar and silver electrodes (599-E; ESL Europe, Berkshire, UK) were screen-printed and dried for 12 h at room temperature. Five tapes were stacked and vacuum-laminated with hot isostatic pressing (75 °C, 80 MPa, 10 min), followed by binder burnout (200−350 °C) and sintering at 450 °C.

2.2. Characterizations. Differential scanning calorimetric (DSC) measurement/thermogravimetric analysis (Netzsch 404 F3, Selb, Germany) at a heating rate of 5 °C/min for samples of 15.4 mg was used to study the burnout of the organic additives. Tensile strength measurements of the green tape were performed using a temperature-controlled tensile strength measurement stage (TST 350, Linkam Scientific Instruments Ltd., Surrey, UK) and Linksys 32 software at room temperature with a speed of 100 μm/s using standard dumbbell-shaped samples (length 36.2 mm and width of 3.1 mm). The crystal structure and bulk density of the sintered specimens were obtained with the X-ray diffractometer (DISCOVER D8, Bruker, Germany) using Cu Kα radiation and Archimedes method, respectively. The microstructure of the sintered sample was studied using field emission scanning electron microscopy (Zeiss Ultra Plus, Germany). The surface roughness of the green and sintered tapes was measured using atomic force microscopy (AFM, Veeco Dimension 3100 SPM). Relative permittivity (ε_r), dielectric loss (tan δ), and capacitance were measured at low frequencies using a precision LCR meter (HP 4284A, Keysight Technologies, USA).

The sintered and electrode-coated PZ29−glass substrate was machined for capacitance measurements using a laser. Microwave dielectric properties of the green and sintered multilayer were measured using the split-post dielectric resonator (SPDR) (QWED, Poland) technique with a vector network analyzer (10 MHz to 20 GHz, Rohde & Schwarz, ZVB20, Germany). The total uncertainty in measuring the relative permittivity was about 0.5% with a possibility to measure dielectric loss in the range of 10^{-5} by the SPDR.[26] The temperature dependence of the microwave dielectric properties was measured using a furnace (Espec SU-261) operating at −40 to 100 °C integrated with a microwave measurement setup. Piezoelectric and ferroelectric properties were measured using the direct piezoelectric response in a piezo d_{33} test system (APC International, Ltd, USA) and ferroelectric tester (Precision LC, Radiant Technologies, USA). The linear coefficient of thermal expansion (CTE) was investigated in the temperature range of 100−425 °C with cylindrical samples of 8 mm × 15 mm^2 using a dilatometer (NETZSCH DIL 402 PC/4, Germany).

3. RESULTS AND DISCUSSION

3.1. Casting and Analysis. In tape casting, the knowledge of the particle size and specific surface area of the starting ceramic powder is crucial for good quality, strong, and flexible green tapes.[27,28] In general, powders with uniform particle size distribution and a surface area of 1−15 m^2/g are required for the tape casting process,[27,29] enabling an optimized slurry composition. The particle size and specific surface area of the

DOI: 10.1021/acsami.8b00978
ACS Appl. Mater. Interfaces XXXX, XXX, XXX−XXX

milled PZ29−glass powder were 6.6 μm and 1.0 m^2/g, respectively. The optimized slurry composition for the tape casting (Table 1) contained 50 wt % of PZ29−glass powder,

Table 1. Optimized Slurry Composition for Tape Casting

materials	compositions (wt %)
PZ29−glass	50
DMC—dimethyl carbonate	43.5
QPAC40	4.3
butyl benzyl phthalate	1.1
polyethylene glycol	1.1

43.5 wt % of DMC as the solvent, and 4.3 wt % of QPAC40 as the binder because of their low burnout temperature (peak rate of decomposition at 230−260 °C).[30] The amount of both plasticizers, butyl benzyl phthalate (BBP) and polyethylene glycol (PEG), was 1.1 wt %.

The surface quality and mechanical properties of the green tapes are the critical parameters which control the postprocessing stages such as the screen printing of the top electrode and the multilayer lamination process.[31−34] Figure 2a shows a

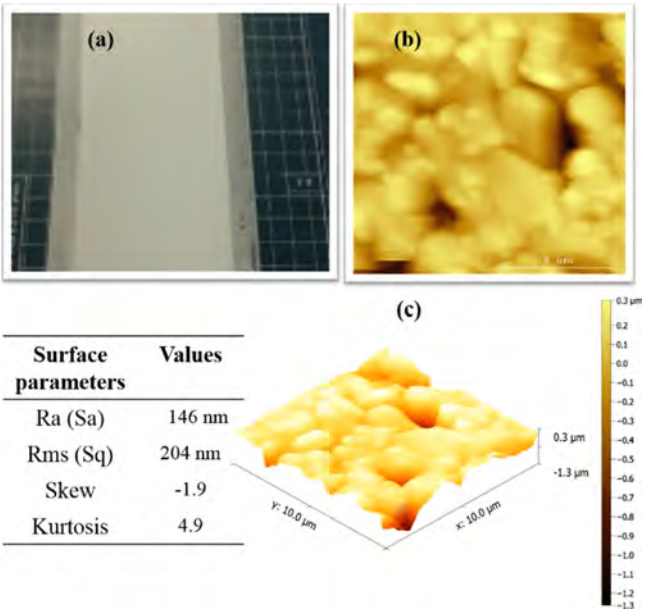

Figure 2. (a) Photograph of the cast green tape and (b,c) AFM 2D and 3D images of the surface of the green tape with a table showing the measured surface parameters.

photograph of the dried green tape, whose measured average thickness was in the range of 82−88 μm. The surface roughness of the green tape was 146 nm in the measured area of 10 × 10 μm (Figure 2b,c).

The skew and kurtosis values were −1.9 and 4.9, respectively, meaning that the green tape was planar with more peaks than valleys.[35] The average tensile strength of the cast single green tape was 0.4 MPa with a standard deviation of 0.02, which is slightly lower than that of commercial DuPont 951 tape, for example, which has a value of 1.8 MPa. The detailed green tape tensile strength comparisons of ULTCC and LTCC DuPont 951 are shown in the Supporting Information Table S1a,b, respectively. The poly (propylene carbonate)-based binder system had a lower strength than that of other binders used in the tape casting process.[27] This is clearly due to the much lower burn out temperature. However, the developed ULTCC green tape was suitable for multilayer stacking and the screen printing process.

Figure 3a shows the TG/DSC analysis of the green tape from room temperature to 450 °C at a heating rate of 5 °C/min. Initially, up to 150 °C, the weight loss was slow, being totally 0.5% because of moisture desorption and trapped solvent evaporation. After that it increased rapidly until 250 °C, mainly because of the decomposition of carbonates from the organic additives such as the binder (QPAC40) which was reported to happen at around 230−350 °C[30] and the plasticizers (BBP and PEG) present in the green tape.[36] The endothermic and exothermic peaks present in the DSC analysis further confirmed the decomposition of the low-molecular weight binder, plasticizers, and melting of low melting-point glass present in the ULTCC composition. The melting of the glass acts as the liquid phase for the PZ29 ceramics, which happens at around 400−415 °C.[37] On the basis of these results, a sintering profile suitable for the PZ29−glass tape was designed and applied (Figure 3b). The laminated five layer green tape had a thickness of 400 μm. Sintering shrinkages of 12, 13, and 16% in the x, y, and z directions, respectively, were observed, with a densification of 95% and a final thickness of 336 μm.

3.2. Structural and Microstructural Studies. Figure 4 shows the X-ray diffraction pattern of PZ29−glass after sintering at 450 °C with the cubic lead zirconium titanate [standard ICDD card (no: 04-011-2333) of $PbZr_{0.4}Ti_{0.6}O_3$] together with a new phase of $LiAlSiO_4$ reacted from the glass composition. Previous research also reported $LiAlSiO_4$ phase formation close to the present sintering temperature of 450 °C.[38]

Figure 5 shows the cross-sectional microstructure of the (a) sintered five layer laminated tape, (b) Ag cofired at 450 °C, and (c) a back-scattered SEM cross-sectional image for EDS analysis and the accompanying table. All the PZ29 particles (spectrum 11) were completely surrounded by a glassy phase (spectrums 10 and 12), where also a small amount of Si was detected. Figure 5c shows also that the cofired Ag was well-attached to the ULTCC substrate. In addition, the EDS line mapping analysis is provided in the Supporting Information Figure S1a−c for further confirming the no Ag diffusivity in the cofiring at 450 °C. The results confirm that the commercial Ag ink is well-suited for the present ULTCC substrate/package material for the low-temperature fabrication of electronic devices. In addition to this, the microstructure of the green tape is also present in the Supporting Information, Figure S2, which shows that the PZ29−glass particles are surrounded by the organic matrix used in the casting.

The AFM surface parameters estimated from the 2D and 3D images of a sintered PZ29−glass sample are shown in Supporting Information, Figure S3a,b. As compared to the green tape, the average surface roughness increased to the value of ∼355 nm, which is lower or at the same level as that reported for commercial LTCCs.[39] A similar trend was also observed in the rms value while the skewness and kurtosis value were negative, indicating a planar nature as well as a more uniform surface grain and valley of the grain boundaries in the glass matrix. The surface roughness analysis is desirable for substrate/package materials when postfiring of accurate conductive lines is needed or if the application is operating at high frequencies.[40] Importantly, when the surface roughness becomes of the order of the skin depth, the attenuation of transmission lines increases.[41]

DOI: 10.1021/acsami.8b00978
ACS Appl. Mater. Interfaces XXXX, XXX, XXX−XXX

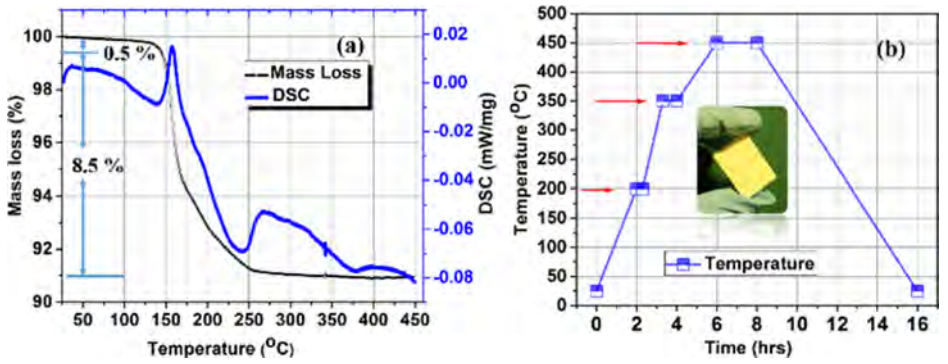

Figure 3. (a) TG and DSC curves of the green tape and (b) optimized sintering profile for PZ29−glass tape with the inset showing the sintered ULTCC substrate.

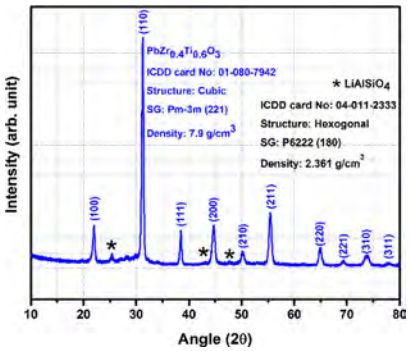

Figure 4. X-ray diffraction pattern of PZ29−glass sintered at 450 °C.

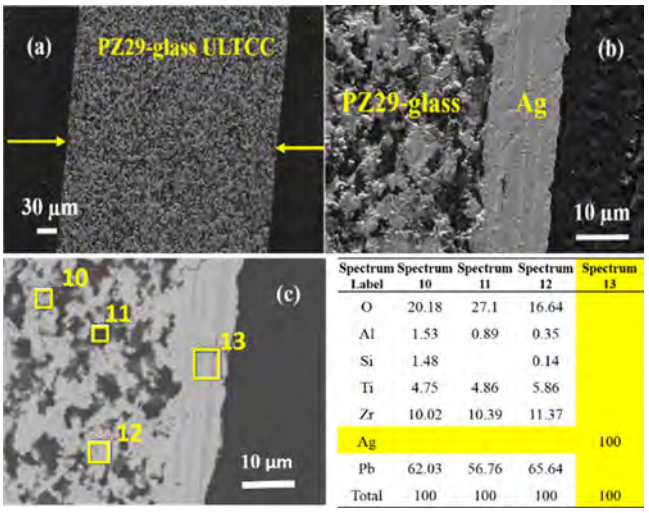

Spectrum Label	Spectrum 10	Spectrum 11	Spectrum 12	Spectrum 13
O	20.18	27.1	16.64	
Al	1.53	0.89	0.35	
Si	1.48		0.14	
Ti	4.75	4.86	5.86	
Zr	10.02	10.39	11.37	
Ag				100
Pb	62.03	56.76	65.64	
Total	100	100	100	100

Figure 5. Cross-sectional microstructure of ULTCC substrate sintered at 450 °C (a) five layer laminated, (b) Ag cofired, and (c) SEM image of Ag cofired substrate with EDS analysis results in the accompanying table.

3.3. Low-Frequency Dielectric Properties of PZ29−Glass Sintered at 450 °C. Figure 6a presents the variation of capacitance with varying frequency up to 1 MHz of the PZ29−glass sintered at 450 °C. It was observed that the developed ULTCC possessed a room-temperature capacitance value of 121 pF measured at 1 MHz. However, most ceramic capacitors are fabricated at a very high sintering temperature such as the LTCC and HTCC ranges. However, ULTCC research is only in the early stages, and more research is needed in this area to enable real practical applications. An alternative option would be the embedding of these capacitors into a module made of different ULTCC compositions. This would be feasible due to the ultralow fabrication temperature.

Figure 6 inset shows the laser-processed SMD ULTCC capacitor prototypes for future electronic applications. Figure 6b reveals the dielectric properties of the ULTCC functional substrate developed before and after the poling process (electric field of 15 V/μm, poling time 5 min with the maximum temperature of 100 °C), which caused about 11% relative permittivity change at 1 MHz and an increase of loss tangent from 0.013 to 0.019. The low relative permittivity value of PZ29−glass is due the low permittivity (~12.8 at 1 MHz) of the commercial glass matrix (44 vol %), although the amount of PZ29 was only 56 vol %.

3.4. Ferroelectric, Energy Storage, and Piezoelectric Studies of Developed Functional ULTCC. The *P*−*E* hysteresis loop and discharge energy of a sample under maximum fields of 10 and 20 V/μm are shown in Figure 6c. The average maximum polarization (P_{max}) and remnant polarization (P_r) were ~2.2 and ~0.8 μC/cm^2, respectively. The developed sample possessed nonlinear polarization and ferroelectric properties with a low value of remnant polarization (0.8 μC/cm^2, at 20 V/μm and 2.5 Hz) as shown in Table 2.

The studied samples did not achieve saturated behavior even at a high electric field (20 V/μm). The low polarization is due to the low coupling of the electric field between the high permittivity ceramic particles and the low permittivity matrix (0−3 connection) as well as the fact that there is only 56 vol % ferroelectric ceramic filler in the material. The maximum electric field that the material could withstand without a breakdown in *PE* measurements was notably higher than that for bulk ceramics, which indicates that the filler particles were well-distributed in the material.[42]

The energy storage properties as described by the energy density (*J*) of the developed ULTCC in an electric field can be calculated by integrating the discharge curve of the *PE*-loop against the polarization (*y*-axis)[43]

$$J = \int E \, dP \tag{1}$$

where *J* is the energy density, *E* is the electric field, and *P* is polarization. The stored energy density (J_s) is equal to the area between the *y*-axis and the charging polarization curve, while the discharge energy (J_d) can be calculated by integrating the area between the discharging polarization curve and the *y*-axis (blue area in Figure 6c). The average energy densities at 10 and 20 V/μm were 0.33 and 0.12 J/cm^3, respectively. The ratio

DOI: 10.1021/acsami.8b00978
ACS Appl. Mater. Interfaces XXXX, XXX, XXX−XXX

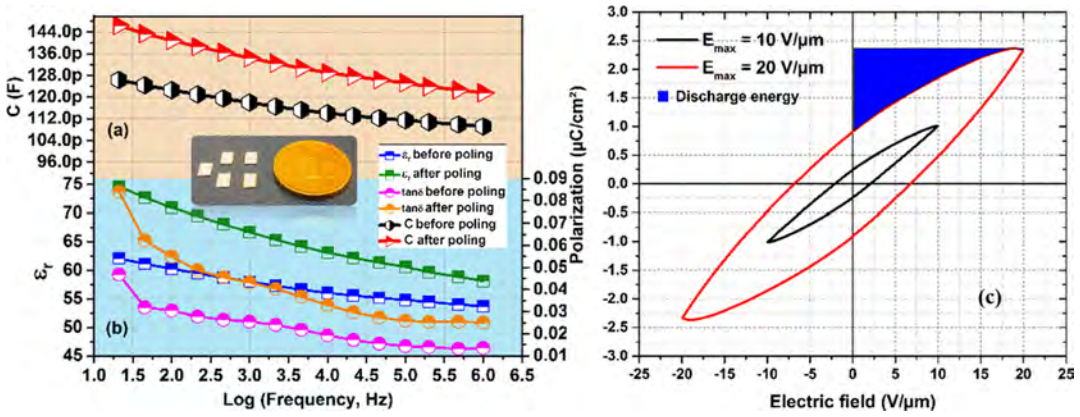

Figure 6. (a,b) Radio frequency dielectric properties before and after the poling process. The Inset photo image shows laser-processed ULTCC functional surface mount device (SMD) capacitors, and (c) PE hysteresis curve at 10 and 20 V/μm maximum fields and discharge energy is shown as blue colored area for 20 V/μm measurement of a multilayer ULTCC sample.

Table 2. Average Ferroelectric Properties with a Standard Deviation of Developed ULTCC PZ29−Glass

ferroelectric properties	P_{max} (μC/cm^2)	P_r (μC/cm^2)	$-P_r$ (μC/cm^2)
average	2.2	0.8	−0.8
standard deviation	5%	∼8.75%	∼8.75%

between these gives an energy efficiency of 36.2%. This low level of efficiency can be understood as being due to the hysteresis losses of the ferroelectric filler and the interfacial polarization.

The low permittivity matrix and high permittivity filler may create extra polarization at the matrix−filler interfaces. These interfacial polarizations have two well-known properties: they increase permittivity at low frequency but decrease the discharged energy in $P-E$ loops due to the longer relaxation time and the trapping of charges at the interfaces[44,45] The unreleased energy can be seen in Figure 6c as the area between the charge and discharge curves. Nevertheless, these results represent the highest values reported for ULTCC materials so far, and they are very comparable with some ceramic−glass capacitor materials (fabrication temperatures > 800 °C).[45,46] Higher energy densities and efficiency could be reached by changing the filler to a material developed for energy storage applications.[47−49]

PZ29 is a piezoelectric material; the PZ29−glass substrate also showed some piezoelectric properties (Table 3) having an

Table 3. The average values of piezoelectric response of the ULTCC multilayer functional Substrate

piezo/dielectric properties	$+d_{33}$ (pC/N)	ε_r @ 1 kHz	tan δ @ 1 kHz	$+g_{33}$ mV/N
average	17.3	65	0.03	30
standard deviation	0.6	1.4	0.004	0.5

average d_{33} of 17.3 pC/N at 110 Hz (the excitation frequency of the piezometer). The estimated voltage coefficient ($+g_{33}$) was 30 mV/N (at 1 kHz), which indicated that the developed material could also be suitable for sensor applications with some further research. As for comparison, the g_{33} of PZT thick film fired on LTCC (ε_r at 1 kHz 195, d_{33} 30 pC/N) and alumina (ε_r at 1 kHz 521, d_{33} 120 pC/N) substrates is 17 and 26 mV/N, respectively.[50] The g_{33} of the bulk PZ29 is reported to be 23 mV/N, which is lower than that calculated with the developed glass substrate. The low g_{33} value of the PZ29 is due to its high permittivity (2900 at 1 kHz). However, it must be kept in mind that the d_{33} of PZ29 is as high as 575.[51]

3.5. Microwave Dielectric Properties of Green Tape and Sintered Substrates. To study the shelf life of the green tape, its dielectric properties were measured as a function of storage time, which indicated the stability of the developed slurry composition. After casting, the green tape showed a relative permittivity of 12.8 and 12.5 and dielectric loss of 0.07 and 0.08, respectively at 2.4 and 5.1 GHz (Supporting Information, Table S2). The difference compared to the sintered multilayer substrate, having a permittivity and dielectric loss of 57.8 and 0.05, respectively, at 2.4 GHz, is due to the organic additives present in the green tape. However, the sintered multilayer substrate did not show resonance at 5.1 GHz, and hence the values were not accessible.

The shelf life of the green single layer tape in terms of its microwave dielectric properties at 2.4 and 5.1 GHz is shown in Supporting Information, Figure S4. The ageing measured over 28 months (Figure S4) showed only about a 0.3−0.4% variation in the relative permittivity and 10% variation in the dielectric loss measured at 2.4 and 5.1 GHz, respectively. The relative permittivity and dielectric loss error bars are assigned based on the SPDR accuracy as well as the calibration at different intervals of time. These results are important to describe the predicted shelf life of ULTCC tape for long-term storage and usages. However, the mechanical properties of the tapes as a function of storage time need further research.

Figure 7 shows the temperature dependence of relative permittivity and dielectric loss of sintered substrate at 2.4 GHz. The relative permittivity increased with increase in the temperature range while the dielectric loss showed an abnormal variation, which was expected and may be due to the high interaction of thermal vibrations on its electronic/ionic polarization in the microwave frequency range. The sintered ULTCC substrate showed a variation of relative permittivity of about 23% in the temperature range of −40 to 90 °C. The dielectric loss value was linear fitted to estimate the approximate temperature variation in dielectric loss at microwave frequency. The dielectric loss also increased with increase in temperature as expected.

The present studies reveal that the ULTCC technology opens up a new path for low-cost fabrication of multilayer packages/substrates fabrication at 450 °C, which is much closer

DOI: 10.1021/acsami.8b00978
ACS Appl. Mater. Interfaces XXXX, XXX, XXX−XXX

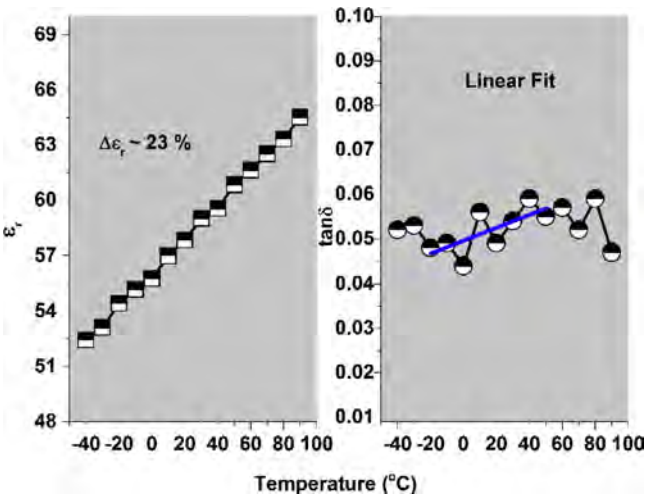

Figure 7. Sintered ULTCC substrate temperature dependence of relative permittivity and dielectric loss at 2.4 GHz.

to room temperature than that of HTCC or LTCC technologies.

3.6. Linear Coefficient of Thermal Expansion of the Sintered PZ29−Glass at 450 °C. Figure 8a,b shows the

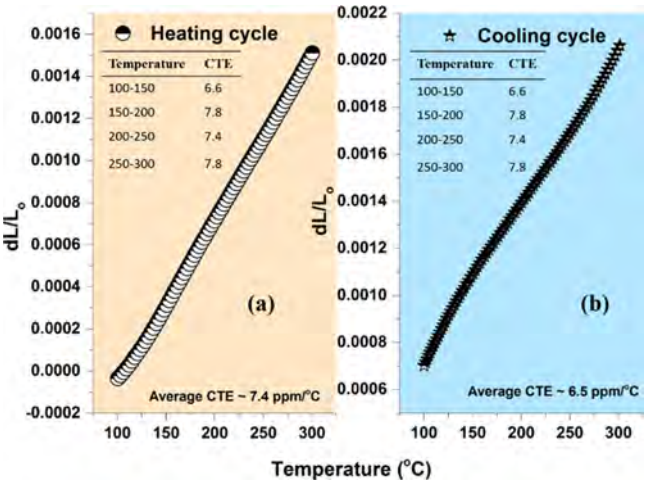

Figure 8. Variation of linear change in dimension with respect to temperature (100−300 °C) of PZ29−glass sintered at 450 °C (a) heating cycle and (b) cooling cycle.

variation of linear change in dimensions within the temperature range [(a) heating and (b) cooling cycle] of 100−300 °C. The calculated linear CTE of 7.4 ppm/°C was observed in the heating cycle (100−300 °C) of the measured temperature ranges. The cooling cycle (300−100 °C) showed a similar trend with an average linear CTE of 6.5 ppm/°C. The variations of linear CTE of the ULTCC sample at selected temperature ranges in the heating and cooling cycle were also calculated and are shown in the inset tables of Figure 8.

The CTE plays an important role in the device level integration, especially during cofiring of two materials. In multilayer structures controlling thermal delamination is one of the major challenge. In order to control the thermal delamination when cofiring, the CTE matching with metals is needed.[21,34] Careful selection of commercial grade Ag paste having the same firing temperature as the developed ULTCC was done. Both of the materials being in a soft stage during the firing minimize problems caused by the CTE difference. The feasibility of the selected Ag paste in this sense was also evident from the microstructure (Figure 5c).

4. CONCLUSION

The present paper reports a new strategy for multifunctional materials through the ULTCC technology. A low-cost fabrication method for new functional ULTCC multilayer structures cofired with Ag at 450 °C and possessing moderate dielectric, piezoelectric, and ferroelectric properties for future low-cost multilayer packages was demonstrated for the first time. The developed PZ29−glass was cast in green tape using a binder system and cofired below 500 °C. A systematic sintering profile was optimized based on the TG-DSC analysis and produced a uniform microstructure and 95% densification. The sintered ULTCC substrate had a low surface roughness (355 nm). The measured voltage coefficient ($+g_{33}$) was 30 mV/N (at 1 kHz), which indicates that the developed material could be feasible for some sensor applications with further research. At microwave frequencies (2.4 GHz), the substrate showed a relative permittivity of 57.8 and a dielectric loss of 0.05. Moreover, the sintered PZ29−glass material exhibited an average linear CTE of 6.9 ppm/°C in the measured temperature range of 100−300 °C. The stability of the green tape as a function of storage time through dielectric properties was also briefly studied, which is an important parameter for commercial fabrication. The results reveal an important step on the way to future multilayer ULTCC production.

■ ASSOCIATED CONTENT

Supporting Information

The Supporting Information is available free of charge on the ACS Publications website at DOI: 10.1021/acsami.8b00978.

(a) Tensile strength of cast green tape with the polycarbonate-based binder system, Table S1(b) tensile strength of commercial DuPont 951 tape, and the microwave dielectric properties of green single tape and four layer isostatic laminated tapes; EDS line-mapping analysis of ULTCC with Ag electrode cofired at 450 °C; SEM microstructure of green tape surface (a,b) magnified image; AFM image of (a) 2D and (b) 3D with the inset table of surface parameters, of a sintered PZ29−glass; and ageing effect of microwave dielectric properties of ULTCC single layer green tape at 2.4 and 5.1 GHz (PDF)

■ AUTHOR INFORMATION

Corresponding Author

*E-mail: jobin.var@gmail.com. Phone: +358-0449141866.

ORCID

Jobin Varghese: 0000-0003-3985-9181

Notes

The authors declare no competing financial interest.

■ ACKNOWLEDGMENTS

Authors are grateful to European Research Council Project no: 24001893 for the financial support. J.V. is thankful to Ulla Tuominen Foundation project grant 2018.

DOI: 10.1021/acsami.8b00978
ACS Appl. Mater. Interfaces XXXX, XXX, XXX−XXX

ABBREVIATIONS

ULTCC, ultra-low temperature co-fired ceramics; LTCC,, low-temperature co-fired ceramics; HTCC,, high temperature co-fired ceramics; SPDR, split-post dielectric resonator; AFM, atomic force microscopy; CTE, coefficient of thermal expansion; ppm, parts per million; SEM, scanning electron microscopy; SMD, surface mound device; TG, thermogravimetric; DSC, differential scanning calorimetric; BBP, butyl benzyl phthalate; PEG, polyethylene glycol

REFERENCES

(1) Tummala, R. R.; Rymaszewski, E. J.; Klopfenstein, A. G. *Microelectronics Packaging Handbook*; Springer US, 1997.

(2) Imanaka, Y. *Multilayered Low Temperature Cofired Ceramics Technology*; Springer: Japan, 2005.

(3) Tummala, R. R. Ceramic and Glass-Ceramic Packaging in the 1990s. *J. Am. Ceram. Soc.* **1991**, *74*, 895−908.

(4) Sobociński, M.; Zwierz, R.; Juuti, J.; Jantunen, H.; Golonka, L. Electrical and Electromechanical Characteristics of LTCC Embedded Piezoelectric Bulk Actuators. *Adv. Appl. Ceram.* **2010**, *109*, 135−138.

(5) Gebhardt, S.; Partsch, U.; Schönecker, A. PZT Thick Films for MEMS. *IEEE International Symposium on Applications of Ferroelectrics*, 2008; Vol. 2.

(6) Joseph, N.; Varghese, J.; Siponkoski, T.; Teirikangas, M.; Sebastian, M. T.; Jantunen, H. Glass-Free $CuMoO_4$ Ceramic with Excellent Dielectric and Thermal Properties for Ultra-Low Temperature Cofired Ceramic Applications. *ACS Sustainable Chem. Eng.* **2016**, *4*, 5632−5639.

(7) Varghese, J.; Siponkoski, T.; Teirikangas, M.; Sebastian, M. T.; Uusimäki, A.; Jantunen, H. Structural, Dielectric, and Thermal Properties of Pb Free Molybdate Based Ultralow Temperature Glass. *ACS Sustainable Chem. Eng.* **2016**, *4*, 3897−3904.

(8) Varghese, J.; Siponkoski, T.; Nelo, M.; Sebastian, M. T.; Jantunen, H. Microwave Dielectric Properties of Low-Temperature Sinterable α-MoO_3. *J. Eur. Ceram. Soc.* **2018**, *38*, 1541−1547.

(9) Chen, M.-Y.; Juuti, J.; Hsi, C.-S.; Chia, C.-T.; Jantunen, H. Dielectric $BaTiO_3$−BBSZ Glass Ceramic Composition with Ultra-Low Sintering Temperature. *J. Eur. Ceram. Soc.* **2015**, *35*, 139−144.

(10) Chen, M.-Y.; Juuti, J.; Hsi, C.-S.; Chia, C.-T.; Jantunen, H. Dielectric Properties of Ultra-Low Sintering Temperature Al_2O_3-BBSZ Glass Composite. *J. Am. Ceram. Soc.* **2015**, *98*, 1133−1136.

(11) Chen, M.-Y.; Vahera, T.; Hsi, C.-S.; Sobocinski, M.; Teirikangas, M.; Peräntie, J.; Juuti, J.; Jantunen, H. Tape Casting System for ULTCCs to Fabricate Multilayer and Multimaterial 3D Electronic Packages with Embedded Electrodes. *J. Am. Ceram. Soc.* **2017**, *100*, 1257−1260.

(12) Sebastian, M. T.; Wang, H.; Jantunen, H. Low Temperature Co-Fired Ceramics with Ultra-Low Sintering Temperature: A Review. *Curr. Opin. Solid State Mater. Sci.* **2016**, *20*, 151−170.

(13) Sebastian, M. T.; Jantunen, H. High Temperature Cofired Ceramic (HTCC), Low Temperature Cofired Ceramic (LTCC), and Ultralow Temperature Cofired Ceramic (ULTCC) Materials. *Microwave Materials and Applications*; John Wiley & Sons Ltd., 2017; Vol. *1*, Chapter 8.

(14) Zhao, S.; Jiang, B.; Maeder, T.; Muralt, P.; Kim, N.; Matam, S. K.; Jeong, E.; Han, Y.-L.; Koebel, M. M. Dimensional and Structural Control of Silica Aerogel Membranes for Miniaturized Motionless Gas Pumps. *ACS Appl. Mater. Interfaces* **2015**, *7*, 18803−18814.

(15) Valant, M.; Popović, J.; Mihelj, M. V.; Burazer, S.; Altomare, A.; Moliterni, A. Oxide Crystal Structure with Square-Pyramidally Coordinated Vanadium for Integrated Electronics Manufactured at Ultralow Processing Temperatures. *ACS Sustainable Chem. Eng.* **2017**, *5*, 5662−5668.

(16) Zhou, D.; Li, W.-B.; Guo, J.; Pang, L.-X.; Qi, Z.-M.; Shao, T.; Xie, H.-D.; Yue, Z.-X.; Yao, X. Structure, Phase Evolution, and Microwave Dielectric Properties of $(Ag_{0.5}Bi_{0.5})(Mo_{0.5}W_{0.5})O_4$ Ceramic with Ultralow Sintering Temperature. *Inorg. Chem.* **2014**, *53*, 5712−5716.

(17) Zhu, X.; Wang, Z.; Su, X.; Vilarinho, P. M. New Cu_3TeO_6 Ceramics: Phase Formation and Dielectric Properties. *ACS Appl. Mater. Interfaces* **2014**, *6*, 11326−11332.

(18) Udovic, M.; Valant, M.; Suvorov, D. Dielectric Characterisation of Ceramics from the TiO_2−TeO_2 System. *J. Eur. Ceram. Soc.* **2001**, *21*, 1735−1738.

(19) Kähäri, H.; Ramachandran, P.; Juuti, J.; Jantunen, H. Room-Temperature-Densified Li_2MoO_4 Ceramic Patch Antenna and the Effect of Humidity. *Int. J. Appl. Ceram. Technol.* **2016**, *14*, 50−55.

(20) Joseph, N.; Varghese, J.; Teirikangas, M.; Sebastian, M. T.; Jantunen, H. Ultra-low sintering temperature ceramic composites of $CuMoO_4$ through Ag_2O addition for microwave applications. *Composites, Part B* **2018**, *141*, 214−220.

(21) Uchino, K. *Ferroelectric Devices & Piezoelectric Actuators*; DEStech Publication Inc., 2017.

(22) Heinonen, E.; Juuti, J.; Jantunen, H. Characteristics of Piezoelectric Cantilevers Embedded in LTCC. *J. Eur. Ceram. Soc.* **2007**, *27*, 4135−4138.

(23) Corker, D. L.; Whatmore, R. W.; Ringgaard, E.; Wolny, W. W. Liquid-Phase Sintering of PZT Ceramics. *J. Eur. Ceram. Soc.* **2000**, *20*, 2039−2045.

(24) Gowdhaman, P.; Antonyraj, K.; Annamalai, V. An Effective Approach on Physical and Dielectric Properties of PZT-PVDF Composites. *Int. J. Adv. Sci. Res.* **2015**, *1*, 322−328.

(25) Siponkoski, T.; Nelo, M.; Palosaari, J.; Peräntie, J.; Sobocinski, M.; Juuti, J.; Jantunen, H. Electromechanical Properties of PZT/P(VDF-TrFE) Composite Ink Printed on a Flexible Organic Substrate. *Composites, Part B* **2015**, *80*, 217−222.

(26) Krupka, J.; Gregory, A. P.; Rochard, O. C.; Clarke, R. N.; Riddle, B.; Baker-Jarvis, J. Uncertainty of Complex Permittivity Measurements by Split-Post Dielectric Resonator Technique. *J. Eur. Ceram. Soc.* **2001**, *21*, 2673−2676.

(27) Mistler, R. E.; Twiname, E. R. *Tape Casting: Theory and Practice*; The American Ceramic Society: 735 Ceramic Place, Westerville, Ohio 43081, 2000.

(28) Liu, Z.; Wang, Y.; Li, Y. Combinatorial Study of Ceramic Tape-Casting Slurries. *ACS Comb. Sci.* **2012**, *14*, 205−210.

(29) Jantunen, H.; Hu, T.; Uusimäki, A.; Leppävuori, S. Tape Casting of Ferroelectric, Dielectric, Piezoelectric and Ferromagnetic Materials. *J. Eur. Ceram. Soc.* **2004**, *24*, 1077−1081.

(30) Gerrit, A.; Luinstra; Borchardt, E. Material Properties of Poly(Propylene Carbonates). *Adv. Polym. Sci.* **2012**, *254*, 29−48.

(31) Abhilash, P.; Sebastian, M. T.; Surendran, K. P. Glass Free, Non-Aqueous LTCC Tapes of $Bi4(SiO_4)_3$ with High Solid Loading. *J. Eur. Ceram. Soc.* **2015**, *35*, 2313−2320.

(32) Roshni, S. B.; Sebastian, M. T.; Surendran, K. P. Can Zinc Aluminate-Titania Composite Be an Alternative for Alumina as Microelectronic Substrate? *Sci. Rep.* **2017**, *7*, 40839.

(33) Rajesh, S.; Jantunen, H.; Letz, M.; Pichler-Willhelm, S. Low Temperature Sintering and Dielectric Properties of Alumina-Filled Glass Composites for LTCC Applications. *Int. J. Appl. Ceram. Technol.* **2012**, *9*, 52−59.

(34) Arun, S.; Sebastian, M. T.; Surendran, K. P. $Li_2ZnTi_3O_8$ Based High κ LTCC Tapes for Improved Thermal Management in Hybrid Circuit Applications. *Ceram. Int.* **2017**, *43*, 5509−5516.

(35) Raposo, M.; Ferreira, Q.; Ribeiro, P. A. A Guide for Atomic Force Microscopy Analysis of Soft-Condensed Matter. *Modern Research and Educational Topics in Microscopy*; Formatex, 2007; 758−769.

(36) Induja, I. J.; Abhilash, P.; Arun, S.; Surendran, K. P.; Sebastian, M. T. LTCC Tapes Based on Al_2O_3−BBSZ Glass with Improved Thermal Conductivity. *Ceram. Int.* **2015**, *41*, 13572−13581.

(37) SCOTT AG. *SCHOTT Technical Glasses Physical and Technical Properties*, 2007 (accessed on Jan 17, 2018).

(38) Koseva, I. I.; Tzvetkov, P. T.; Yordanova, A. S.; Marychev, M. O.; Dimitrov, O. S.; Nikolov, V. S. Preparation of Chromium Doped $LiAlSiO_4$ Glass-Ceramics. *Bulg. Chem. Commun.* **2017**, *49*, 366−370.

DOI: 10.1021/acsami.8b00978
ACS Appl. Mater. Interfaces XXXX, XXX, XXX−XXX

(39) Dupont. *DuPont GreenTape: Design and Layout Guidelines, 2009*, 12. (accessed on Jan 17, 2018).
(40) Rajesh, K. B.; Subba, R. T. AFM Studies on Surface Morphology, Topography and Texture of Nanostructured Zinc Aluminum Oxide Thin Films. *Dig. J. Nanomater. Biostructures* **2012**, *7*, 1881−1889.
(41) Hammerstad, E. O.; Bekkadal, F. *A Microstrip Handbook*; University of Trondheim: Norway, 1975.
(42) Wang, X.; Zhang, Y.; Song, X.; Yuan, Z.; Ma, T.; Zhang, Q.; Deng, C.; Liang, T. Glass Additive in Barium Titanate Ceramics and Its Influence on Electrical Breakdown Strength in Relation with Energy Storage Properties. *J. Eur. Ceram. Soc.* **2012**, *32*, 559−567.
(43) Herczog, A. Application Of Glass-Ceramics For Electronic Components And Circuits. *IEEE Trans. Parts, Hybrids, Packag.* **1973**, *9*, 247−256.
(44) Hao, X. A Review on the Dielectric Materials for High Energy-Storage Application. *J. Adv. Dielectr.* **2013**, *3*, 1330001.
(45) Zhang, Y.; Huang, J.; Ma, T.; Wang, X.; Deng, C.; Dai, X. Sintering Temperature Dependence of Energy-Storage Properties in (Ba,Sr)TiO_3 Glass-Ceramics. *J. Am. Ceram. Soc.* **2011**, *94*, 1805−1810.
(46) Patel, S.; Chauhan, A.; Kundu, S.; Madhar, N. A.; Ilahi, B.; Vaish, R.; Varma, K. B. R. Tuning of Dielectric, Pyroelectric and Ferroelectric Properties of $0.715Bi_{0.5}Na_{0.5}$ TiO_3-$0.065BaTiO_3$-$0.22SrTiO_3$ Ceramic by Internal Clamping. *AIP Adv.* **2015**, *5*, 087145.
(47) Wang, H.; Liu, J.; Zhai, J.; Shen, B.; Pan, Z.; Liu, J. R.; Yang, K. Effect of Crystallization Temperature on Dielectric and Energy-Storage Properties in SrO-Na_2O-Nb_2O_5-SiO_2 Glass-Ceramics. *Ceram. Int.* **2017**, *43*, 8898−8904.
(48) Zhang, W.; Wang, J.; Xue, S.; Liu, S.; Shen, B.; Zhai, J. Effect of La_2O_3 Additive on the Dielectric Properties of Barium Strontium Titanate Glass−Ceramics. *J. Mater. Sci.: Mater. Electron.* **2014**, *25*, 4145−4149.
(49) Chen, K.; Pu, Y.; Xu, N.; Luo, X. Effects of SrO−B_2O_3−SiO_2 Glass Additive on Densification and Energy Storage Properties of $Ba_{0.4}Sr_{0.6}TiO_3$ Ceramics. *J. Mater. Sci.: Mater. Electron.* **2012**, *23*, 1599−1603.
(50) Hrovat, M.; Belavič, D.; Uršič, H.; Kita, J.; Holc, J.; Drnovšek, S.; Cilenšek, J.; Kosec, M.; Moos, R. An Investigation of Thick-Film Materials for Temperature and Pressure Sensors on Self-Constrained LTCC Substrates. *Proceedings—2008 2nd Electronics System-Integration Technology Conference (ESTC)*, 2008; pp 339−345.
(51) Ferroperm. *High Quality Components and Materials for the Electronic Industry* (accessed on Jan 17, 2018).

DOI: 10.1021/acsami.8b00978
ACS Appl. Mater. Interfaces XXXX, XXX, XXX−XXX